

Ion Solvation in Supercritical Water Based on an Adsorption Analogy

Lewis W. Flanagan,[†] Perla B. Balbuena,^{†,§} Keith P. Johnston,^{*,†} and Peter J. Rossky^{*,‡}

Departments of Chemical Engineering, Chemistry, and Biochemistry The University of Texas at Austin, Austin, Texas 78712

Received: March 11, 1997; In Final Form: July 24, 1997[®]

The solvation structure and free energy for Li^+ , Na^+ , K^+ , F^- , Cl^- , Be^{2+} , Mg^{2+} , and Ca^{2+} in supercritical aqueous solutions are described by a dielectric concentric shell model incorporating solvent adsorption analogous to a Langmuir model. The ratio of solvent bulk density to the local density in the first coordination shell of alkali and halide ions obtained from molecular dynamics simulation is shown to be linear in bulk density at supercritical temperatures, justifying the model. The model utilizes two parameters: a maximum local density, which is found to be insensitive to temperature and correlated with the surface field, and a desorption constant, which we find may be approximated as zero in the free energy calculations. In comparison to the Born model, free energies of solvation predicted by the concentric shell model show far better agreement with values from full molecular simulation and with those from a compressible continuum model.

1. Introduction

In 1920 Born¹ calculated the work or free energy required to transfer a spherical particle of charge q and radius a from a vacuum to a solvent with dielectric constant ϵ :

$$\Delta A^{\text{solv}} = -\frac{\eta q^2}{2a} \left(1 - \frac{1}{\epsilon}\right) \quad (1)$$

where $\eta = 332.054 \text{ Å kcal/mol}$ when q is expressed in elementary charges. Although ambient water is comprised of nonspherical, polar molecules that exhibit hydrogen bonding, the Born model or analogous continuum descriptions have often been successful for hydration thermodynamics.^{2–5} To date, models for aqueous solutions at temperatures above 325 °C have tended to be even more empirical⁶ or have been applied to calculate phase equilibria but not free energies of solvation for ions.⁷ For supercritical water (SCW), widely used programs such as SUPCRT92⁸ employ the Born model as the basis for calculations with empirical correction terms added as needed. Alternatively, ion hydration models in which solvent molecules nearest the ion are treated discretely while the remainder are treated as a continuum, so-called semicontinuum models, have been considered. Such models have been applied to water over a wide range of temperatures and pressures. Most of these have involved incorporating a distance-dependent dielectric function.^{9–17} In particular, solvation free energies have been calculated in supercritical water with the semicontinuum model of Tanger and Pitzer,¹⁸ which includes an empirical effective Born radius and an empirical parameter that represents the effective volume increment for each water of hydration. This model was extended to include hydrogen bonds between the first-shell water molecules and additional water molecules in the bulk.¹⁹ For solutes of arbitrary shape, free energies may be calculated within a continuum picture via a finite-difference numerical solution to Poisson's equation, such as implemented in the program DelPhi,⁵ and this has been utilized recently for solutes in SCW.^{20–23}

An adsorption picture has been found to be a useful description as well. Kajimoto et al.²⁴ first described the aggregation of solvent molecules about a nonionic solute in a supercritical fluid in terms of Langmuir adsorption equilibria. Recently, Subramanian et al.²⁵ explicitly determined clustering (local density augmentation) of carbon dioxide molecules around naphthalene by adaptation of their simplified local density (SLD) adsorption model. The SLD model predictions describing clustering phenomena agree fairly well with results inferred from experimental spectroscopic studies.^{26–28} As shown in Figures 3 and 5 of ref 29 and also reflected in the calculated solvation free energy isotherms, the local density enhancement of supercritical water about the chloride ion²⁹ also mimics adsorption phenomena.

Our objective here is to present a semicontinuum model of ion hydration that is based on molecular level studies and avoids the use of empirical parameters, yet agrees reasonably well with free energies from experiment and molecular dynamics computer simulation. Our model is founded on theoretical determinations of local density enhancement of solvent about solute, guided by new computer simulation data. The parameters in the Langmuir model are inferred from simulation data and are used both to extrapolate local density data and to predict the behavior of new systems for which data are not available. For calculation of free energies, the local densities are incorporated into a concentric shell (CS) semicontinuum model, as described in previous work.²³ This approach is extended to solutes of different size and charge, thereby paving the way for a predictive method of obtaining local densities for use in the CS method of calculating solvation free energies.

To produce the most useful results in the near-critical region from 350 to 450 °C, our model is based on the Helmholtz free energy (whose natural variables are temperature and density), rather than the Gibbs free energy (whose natural variables are temperature and pressure). The solvation by water in this regime is characterized much more directly by solvent density than by pressure. A Helmholtz free energy model can be used equally well to determine chemical potentials or fugacities required for chemical equilibrium and phase equilibrium calculations.

In the final section of this paper, dielectric profiles and free energies predicted by the compressible continuum model^{12,13} are discussed and compared to properties derived from molecular dynamics simulations and the CS model. This compressible

* To whom correspondence should be addressed.

[†] Department of Chemical Engineering.

[‡] Department of Chemistry and Biochemistry.

[§] Present address: Department of Chemical Engineering, The University of South Carolina, Columbia, SC 29208.

[®] Abstract published in *Advance ACS Abstracts*, September 1, 1997.

TABLE 1: Gas-Phase Ion–Water Complex Data and Our Calculated Ion–Oxygen Lennard-Jones Interaction Parameters for SPC/E Water (Distances in Angstroms, Energies in kcal/mol)

ion	R_{IO}^{34}	$\angle \text{IOH}^{34}$	$\Delta H_{\text{IW}}^{34}$	σ_{IO}	ϵ_{IO}
Li^+	1.89	180.0°	−34.0	2.72	0.024
Na^+	2.25	180.0°	−24.0	3.06	0.043
K^+	2.69	180.0°	−17.9	3.93	0.009
F^-	2.51	47.9°	−23.3	3.13	0.137
Cl^-	3.31	37.8°	−13.1	3.55	1.904
Be^{2+}	1.50	180.0°	−140.0	1.43	96.650
Mg^{2+}	1.95	180.0°	−80.0	1.91	35.189
Ca^{2+}	2.40	180.0°	−53.0	2.38	19.560

continuum model has been used previously for spherical ions^{12,13} and was introduced more recently for nonspherical solutes.^{17,21,30} The compressible continuum model has been incorporated into DelPhi, and thermodynamic as well as structural properties have been calculated with the model. For an $\text{S}_{\text{N}}2$ reaction in SCW,³⁰ the results have been shown to agree more closely with our simulations than is found using a simple uniform density continuum approach.²²

2. Methodology

The molecular simulation techniques used to generate solvent density profiles are the same as those described in ref 29. However, the SPC/E potential model of water³¹ is used in the present simulations because of its superior agreement with experimental physical properties of water.^{32,33} The experimental critical properties of water are 647.13 K, 0.322 g/cm³, and 220.55 bar; for comparison, the critical properties of SPC/E water, as estimated by Guissani and Guillot,³² are 640 K, 0.29 g/cm³, and 160 bar. Interactions between an ion and water molecules consist of Coulombic terms plus van der Waals contributions computed via a Lennard-Jones potential. Each pair of ion–water Lennard-Jones parameters is chosen by requiring that the ion–oxygen distance and binding energy for a gas-phase ion complex with a single water molecule agree with the *ab initio* geometry³⁴ and experimental enthalpy of hydration^{35–37} when the orientation is fixed at the *ab initio* value. The Lennard-Jones parameters obtained in this manner as well as the data from which they are derived are displayed in Table 1.

In the molecular simulations, a single ion is placed in a cubic box containing 500 SPC/E water molecules. The canonical ensemble is obtained by resetting the temperature through a velocity resampling every 250 steps. The box length is chosen to give an average density equal to the desired bulk solvent density. Long-ranged forces are computed using the Ewald sum method.^{38,39} After the system is equilibrated for at least 40 ps, data are collected for another 40 ps, where the duration of each time step is 0.002 ps.

Each ion was simulated in water at ambient conditions and at high temperature (673 K ($T_r = 1.05$)) at three different densities: 0.5, 0.29, and 0.087 g/cm³ ($\rho_r = 1.7, 1.0$, and 0.3, respectively). Ion–oxygen and ion–hydrogen radial density distributions and corresponding correlation functions, $g(r)$, were obtained in each case.

3. Results and Discussion

3.1. Molecular Simulations. The sodium cation–water $g(r)$'s at ambient conditions (298 K, 0.997 g/cm³) are illustrated in Figure 1a. These are consistent with the picture of a heavily populated first hydration shell about the cation with the solvated water molecules oriented such that the hydrogen atoms point away from the ion. At ambient conditions, a second peak

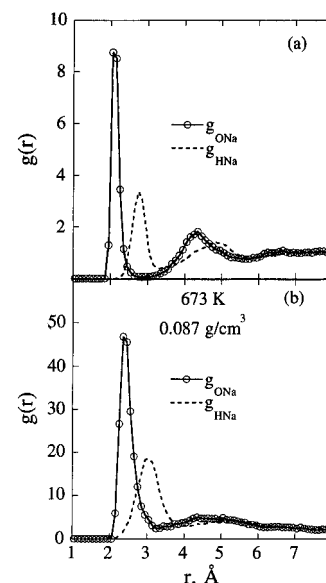


Figure 1. Radial distribution functions of oxygen and hydrogen about Na^+ in (a) ambient water and (b) water at 673 K and 0.087 g/cm³. Note that a and b have different vertical scales.

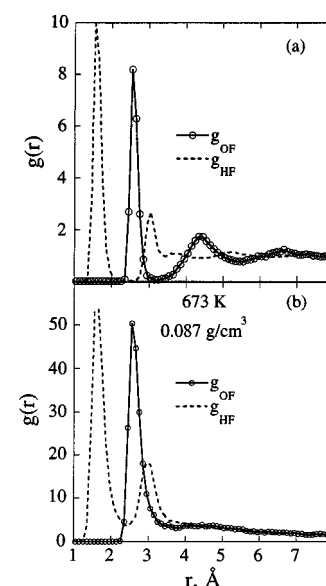


Figure 2. Radial distribution functions of oxygen and hydrogen about F^- in (a) ambient water and (b) water at 673 K and 0.087 g/cm³. Note that a and b have different vertical scales.

somewhat broader than the first is readily seen, which suggests that a second solvation shell, although not as ordered as the primary shell, exists nonetheless. After the second shell, however, the $g(r)$ values level off to the bulk value of 1.

For comparison, results for the ambient fluoride anion–water system are displayed in Figure 2a. The fluoride ion exhibits two first-shell peaks in g_{HF} due to bond-oriented solvation: a very large first peak in g_{HF} closer to the anion than the first peak in g_{OF} , and a second observable peak in g_{HF} , just trailing the first peak in g_{OF} . At these conditions, a second solvation shell is observable in g_{OF} , but a third solvation shell is only slightly detectable.

At 673 K and 0.087 g/cm³ (supercritical conditions), the solvent density about the ion remains high in the vicinity of the ions (Figures 1b and 2b). The primary solvation shell remains largely intact,^{29,40–43} but the density of solvent molecules beyond the primary solvation shell is far more weakly correlated with the presence of the ion. This holds true for all

TABLE 2: Characteristic Features of First Solvation Shells from Ion–Oxygen Radial Distribution Functions. Inner and Outer Boundaries of Shell Denoted by a and b , Respectively. All Distances in Angstroms

(a) 298.15 K, 0.997 g/cm ³								
ion	a	b	peak distance			n_i		
			this work	ref 44	X-ray ⁴⁵	this work	ref 44	X-ray ⁴⁵
Li ⁺	1.55	2.35	1.75	1.95	1.95–2.25	4.0	4.9	4–6
Na ⁺	1.85	2.85	2.05	2.33	2.38, 2.4	4.6	6.0	4, 6
K ⁺	2.45	3.65	2.75		2.8, 2.9	6.7		2–4
F [−]	2.35	3.25	2.55	2.60		6.1	6.2	
Cl [−]	2.82	4.00	3.30	3.21	3.10–3.35	7.4	7.4	4–11
Be ²⁺	1.45	1.75	1.55			4.0		
Mg ²⁺	1.85	2.25	2.05		2.0, 2.1	6.0		6, 8
Ca ²⁺	2.25	3.05	2.45		2.26–2.44	8.1		6–8

(b) 673 K, 0.087 g/cm ³				
ion	a	b	peak distance	n_i
Li ⁺	1.75	2.85	1.95	4.1
Na ⁺	2.05	3.25	2.35	4.8
K ⁺	2.35	3.75	2.75	4.8
F [−]	2.25	3.45	2.55	5.6
Cl [−]	2.82	4.75	3.30	7.5
Be ²⁺	1.45	1.85	1.55	4.0
Mg ²⁺	1.85	2.55	2.05	6.0
Ca ²⁺	2.25	3.25	2.45	8.0

monovalent ionic species, regardless of size; however, the second shell for divalent cations persists to high temperatures, although it is not as prominent as at ambient conditions.⁴³

The key structural features for all of the ions simulated in the present work at ambient conditions and at 673 K and 0.087 g/cm³ are presented in Table 2 (the simulation data for K⁺ are taken from ref 43). In addition to the radial distances at which peaks or shell boundaries occur, an important structural quantity is the coordination number, or number of water molecules within the first solvation shell. The coordination number, n_i , is found by integrating the solvent number density from the inner to the outer boundary of the first solvation shell:

$$n_i = 4\pi\rho_b \int_a^b g_{Oi}(r)r^2 dr \quad (2)$$

Here, ρ_b is the bulk solvent number density, a is the point at which $g(r)$ first rises from zero, and b is the point at which the first minimum in $g(r)$ occurs. Table 2 also shows results from Monte Carlo simulations⁴⁴ performed on ambient dilute aqueous solutions of Li⁺, Na⁺, F[−], and Cl[−] ions using the TIP4P potential of water. The F[−]–water and Cl[−]–water interaction potentials used in these MC simulations were found in the same manner as that described in this work, and the structural quantities obtained for these ions are very similar to our own (Table 2). Small differences between the calculated structural properties for Li⁺ and Na⁺ from ref 44 and our own results may be due to additional constraints which were applied there in determining the Li⁺–water and Na⁺–water interaction potentials. As can be seen from Table 2, the ion–oxygen distances and coordination numbers reported in this work and ref 44 are supported by experimental measurements of these quantities obtained by X-ray diffraction.⁴⁵ Hydration numbers for the Be²⁺ and Mg²⁺ ions found by nuclear magnetic resonance techniques⁴⁶ are 4 and 6, respectively, also in agreement with our simulated values.

Table 2b presents characteristic features of primary solvation shells at 673 K and 0.087 g/cm³. The main effects of this change in state on the first shell are to displace the shell slightly

farther away from the ion (i.e., larger values of a) and to broaden the width of the shell (i.e., larger values of the quantity $b - a$). Notably, the coordination numbers remain remarkably high at this state point, as observed earlier for the chloride ion;^{29,43} even higher temperatures are required to desolvate these ions. Further, at this temperature, the density has almost no effect on the characteristic distances (not shown).

To introduce these structural results into the concentric dielectric shell free energy model of Beveridge and Schnuelle,⁴⁷ hereafter referred to as the CS model, the coordination numbers must be converted into local densities. We use the formula

$$\rho^{\text{loc}} = \frac{n_i m_{\text{H}_2\text{O}}}{V_{\text{shell}}} = \frac{n_i m_{\text{H}_2\text{O}}}{(4/3)\pi(b^3 - a^3)} \quad (3)$$

where $m_{\text{H}_2\text{O}}$ is the mass of a water molecule and V_{shell} is the volume of the first shell. At this point, straightforward application of the method described by Johnston et al.²³ for finding free energies by incorporating local densities in the CS model is possible. However, a means for predicting local densities without performing molecular simulations on each system of interest is desirable. The approach developed in this paper is provided by quantifying a Langmuir adsorption analogy applied to solvation phenomena. The analogy was described qualitatively in ref 29.

3.2. Langmuir Adsorption Analogy. The Langmuir adsorption isotherm may be derived using either statistical mechanics^{48,49} or kinetic rate laws.²⁴ Here we obtain the analogy of local density augmentation to Langmuir adsorption using kinetic rate laws as per Kajimoto et al.²⁴

Let n_i be the number of molecules now being accommodated within the first solvation layer about the ion, i.e., the coordination number. Denote the maximum number of molecules that can be accommodated within this first layer at the given temperature by n_i^{max} . Then, the “fractional coverage” of the first solvation shell, θ , is given by n_i/n_i^{max} . The outgoing rate of solvating molecules is given by $k_o\theta$, where k_o is the outgoing rate constant. The incoming rate is given by $k_i(1 - \theta)\rho$, where k_i is the incoming rate constant and ρ is the (bulk) solvent density outside the shell. At equilibrium, the incoming and outgoing rates should be equal:

$$k_o\theta = k_i(1 - \theta)\rho \quad (4)$$

The local density, ρ^{loc} , within the first solvation shell is proportional to the coordination number, n_i , per eq 3. Hence, the maximum local density at the given temperature is given by

$$\rho^{\text{max}} = n_i^{\text{max}} m_{\text{H}_2\text{O}} / V_{\text{shell}} \quad (5)$$

Substitution of eqs 3 and 5 into eq 4 yields

$$k_o\rho^{\text{loc}}/\rho^{\text{max}} = k_i(1 - \rho^{\text{loc}}/\rho^{\text{max}})\rho \quad (6)$$

Rearrangement of eq 6 into the form

$$\rho/\rho^{\text{loc}} = K(1/\rho^{\text{max}}) + (1/\rho^{\text{max}})\rho \quad (7)$$

suggests that from a plot of the ratio ρ/ρ^{loc} versus ρ one may extract ρ^{max} from the slope and the desorption constant $K \equiv k_o/k_i$ from the intercept. Henceforth, such a plot will be referred to as a Langmuir plot and the quantities ρ^{max} and K as Langmuir constants. Both Langmuir constants have dimensions of density and are given here in units of g/cm³.

Another equation that allows one to see the behavior of ρ^{loc} under various limiting conditions of ρ is the following:

$$\rho^{\text{loc}}/\rho^{\text{max}} = \rho/(K + \rho) \quad (8)$$

In the limit of zero bulk density, the local density also goes to zero. In the limit of $K \rightarrow 0$, ρ^{loc} attains a constant value of ρ^{max} ; that is, the coordination number remains constant regardless of solvent density. (Note that in this study nonzero values for K are used throughout.) In general, smaller values of K imply smaller changes in the coordination number with density.

Using eq 3, local solvent densities about each ion were obtained from the coordination numbers at 673 K and three different densities, and Langmuir plots were generated for each ion. Results are given for K^+ in Figure 3. A linear least-squares regression through the data gives values of 0.80 and 0.031 g/cm^3 for ρ^{max} and K , respectively. As can be judged from the quality of the fit to the data in Figure 3, this system is described very accurately by the Langmuir model. Langmuir constants for the remaining ions are included in Table 3. As is evident from the quality of the regressions (R^2 in Table 3), a linear relationship holds very well for all cases.

If the Langmuir parameters may be correlated with well-known properties of ions, then they may be predicted for new systems without the need to perform new simulations. In Figure 4, the Langmuir parameter ρ^{max} at 673 K (Table 3) is plotted versus the surface field, $|Z|/R_{\text{io}}^2$, where Z is the ionic elementary charge and R_{io} is the ab initio ion–oxygen distance for a gas-phase ion complex with a single water molecule (Table 1). The straight line shown in Figure 4 comes from a linear regression of the data with the fluoride ion excluded for reasons given below. Greater charge/area ratios increase markedly the amount of attraction experienced between the ion and the water molecules since Coulombic forces dominate the dispersive interactions; hence, the overall effect is to increase local density. When all of the ions are considered together as a set, ρ^{max} increases linearly with increasing surface field for all ions except for the fluoride ion. The fluoride ion has a Lennard-Jones diameter roughly the same size as that of the sodium ion, but its local density is significantly enhanced relative to the sodium ion. The atypical behavior of the fluoride ion may be explained by the significant amount of hydrogen bonding in which it engages with water.

The Langmuir desorption constant K is shown for the ions in order of increasing σ_{io} in Table 4. It is apparent that there is no correlation between σ_{io} and K . The table shows that K is usually less than 0.05 g/cm^3 . We believe that this lack of correlation is a reflection of the uncertainty in these values here. According to eq 8, for all ions shown with the exception of fluoride, the maximum error introduced in $\rho^{\text{loc}}/\rho^{\text{max}}$ by setting K equal to zero is 9%, 14%, and 33% for bulk densities of 0.5, 0.3, and 0.1 g/cm^3 , respectively. However, the main concern in this work is the prediction of solvation free energies. The difference introduced by setting $K = 0$ in the value of the solvation free energy calculated using the concentric shell model (section 3.3) is $<1\%$ for bulk densities of 0.5 and 0.3 g/cm^3 and $<1.5\%$ for a bulk density of 0.1 g/cm^3 . Thus, for present purposes, it is adequate to assume a zero value for K , although this was not done.

Thus far in the discussion of the Langmuir adsorption analogy, all comparisons have been made at a single temperature, 673 K, slightly above the critical temperature of pure water. In Figure 5, Langmuir plots for the chloride ion at 673, 768, and 909 K are selected for comparison. Least-squares best-fit lines were drawn through the data at each temperature, and the Langmuir parameters derived from these lines are presented in Table 5. Since the slopes of the three Langmuir lines are almost identical, ρ^{max} remains approximately constant at 0.8

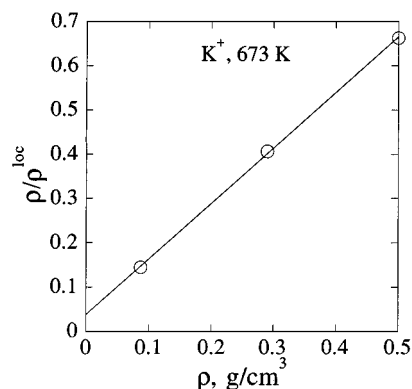


Figure 3. Langmuir plot for K^+ in water at 673 K: (○) simulation (this work and ref 43).

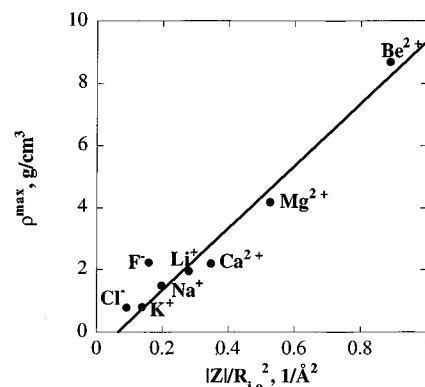


Figure 4. Correlation of maximum local density parameter to surface field.

TABLE 3: Langmuir Parameters (g/cm^3) at 673 K and R^2 Values for the Linear Regression of the Local Density Data from Simulation

ion	ρ^{max}	K	R^2
Li^+	1.96	0.042	0.9597
Na^+	1.49	0.000	0.9918
K^+	0.80	0.031	0.9999
F^-	2.23	0.142	0.9638
Cl^-	0.78	0.027	0.9968
Be^{2+}	8.69	0.000	1.0000
Mg^{2+}	4.19	0.041	0.8994
Ca^{2+}	2.20	0.004	0.9868

TABLE 4: Langmuir Desorption Constant K (g/cm^3) at 673 K for Ions in Order of Increasing Lennard-Jones Diameter (\AA)

ion	σ_{io}	K
Be^{2+}	1.43	0.000
Mg^{2+}	1.91	0.041
Ca^{2+}	2.38	0.004
Li^+	2.72	0.042
Na^+	3.06	0.000
F^-	3.13	0.142
Cl^-	3.55	0.027
K^+	3.93	0.031

g/cm^3 . Therefore, we infer that ρ^{max} may be viewed as a temperature-independent parameter. This is plausible since ρ^{max} is dominated by excluded volume effects, which are not sensitive to temperature. However, the desorption constant K increases steadily with temperature. Since K is the ratio of rate constants for molecules leaving to those entering the first solvation shell, the increase in K with temperature is expected in general. However, we note that even at 909 K, K is small, and assuming $K = 0$ will not introduce significant error into the calculations for solvation free energies described in the following section. In our calculations, we did not assume $K = 0$.

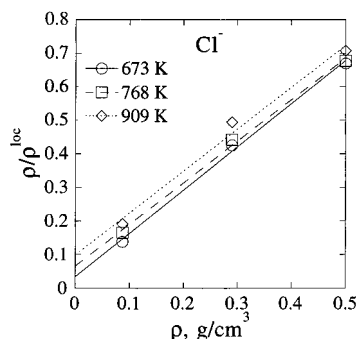


Figure 5. Langmuir plots for Cl^- at three supercritical temperatures.

TABLE 5: Langmuir Parameters (g/cm^3) for the Chloride Ion at Three Supercritical Temperatures (K)

temperature	ρ^{\max}	K
673	0.78	0.027
768	0.81	0.053
909	0.80	0.079

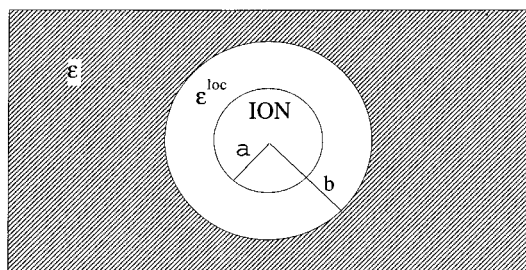


Figure 6. The concentric dielectric shell model.

3.3. Concentric Dielectric Shell Model. Local densities predicted by the Langmuir adsorption analogy of section 3.2 are used now to obtain local dielectric constant values for the first solvation shell of an ion. The values for ρ^{\max} are estimated from Figure 4.

The equation of state method used here for converting local densities to local dielectric values is not new and has been described previously,²³ but here we incorporate the dielectric equation of state $\epsilon = \epsilon(T, \rho)$ adopted by Uematsu and Franck.⁵⁰ The local dielectric value, ϵ^{loc} , is found by substituting the local density, ρ^{loc} , for the bulk density, ρ , in the dielectric equation of state.

In the CS model (Figure 6), the values used here for the inner radius, a , and outer radius, b , of the first solvation shell are given by simulation (Table 2). The charge, q , is assumed to be fixed at the center of the spherical ion. As mentioned previously, the dielectric function, $\epsilon(r)$, varies with radial distance, r , from the center of the ion as follows: $\epsilon(r) = 1$ for $r < a$ (within the ion cavity), $\epsilon(r) = \epsilon^{\text{loc}}(\rho^{\text{loc}}, T)$ for $a < r < b$ (within the first solvation shell), and $\epsilon(r) = \epsilon(\rho, T)$ for $r > b$ (within the bulk solvent). The solution for the solvation free energy for the ion in this system is given by⁴⁷

$$\Delta A^{\text{solv}} = -\frac{\eta q^2}{2} \left\{ \left(\frac{1}{a} - \frac{1}{b} \right) \left(1 - \frac{1}{\epsilon^{\text{loc}}} \right) + \frac{1}{b} \left(1 - \frac{1}{\epsilon} \right) \right\} \quad (9)$$

where $\eta = 332.054 \text{ Å kcal/mol}$. If $b = a$, eq 9 clearly reduces to the Born equation (eq 1). As noted in ref 23, the results are reasonably sensitive to a , but are insensitive to the precise choice of b . The molecular simulations to obtain radial distribution functions from which the inner radius a is found are quite simple and short compared to those used in the free energy perturbation calculations. In addition, values of a are already known for most atomic ions. Simulations are not required to obtain a ,

TABLE 6: $-\Delta A^{\text{solv}}$ Predicted by the CS Model. Experimental Values at Ambient Conditions⁶⁰ Are Shown at the Top for Comparison. ρ in g/cm^3 , T in K, $-\Delta A^{\text{solv}}$ in kcal/mol

ρ	T	ϵ	Li^+	Na^+	K^+	F^-	Cl^-	Ca^{2+}
experimental								
0.997	298	78.24	122.1	98.2	80.6	103.8	75.8	380.8
CS model								
0.997	298	78.24		88.68	66.98	69.79	58.17	
0.500	673	9.93	99.95	83.48	65.16	68.30	54.03	272.88
0.350	673	6.10	84.89	79.79	62.57	65.56	51.74	261.33
0.290	673	4.83	82.38	77.41	61.18	63.42	50.11	253.29
0.087	673	1.74	60.68	50.91	45.00	45.54	37.09	173.70
0.014	673	1.10	37.91	33.73	24.99	21.92	21.59	106.88
0.500	768	8.60	98.64	82.48	64.00	67.40	53.26	266.63
0.350	768	5.31	83.27	78.26	61.27	64.29	50.68	253.39
0.290	768	4.23	80.58	75.56	59.17	62.03	48.97	244.16
0.014	768	1.08	36.72	33.05	23.62	20.46	20.49	104.19
0.500	909	7.41	94.70	80.92	62.88	65.55	52.32	271.34
0.350	909	4.63	80.15	76.18	59.74	62.45	49.41	256.86
0.014	900	1.07	35.43	32.06	22.19	18.95	19.33	110.06

however, because the parameter a may be estimated from experimental data by approximating a as $R_{\text{io}} - \delta$, where δ is a measure of the distance between the minimum in the potential well and the steep potential wall; in essence, a may be determined from the potential energy curve alone. From Tables 1 and 2, it is evident that δ is not very state dependent and increases slightly with σ_{io} . From comparing R_{io} from Table 1 to a from Table 2, it is seen that δ is approximately 0.3 Å for monovalent atomic ions and 0.1 Å for divalent atomic ions.

The solvation free energies predicted by the CS model for the ions in Table 2 at 13 state conditions are shown in Table 6. Data for Be^{2+} and Mg^{2+} under all conditions and Li^+ and Ca^{2+} under ambient conditions are excluded due to the effect of large local densities predicted by the Langmuir model. The dielectric equation of state for water is untenable for these conditions because the local densities are much higher than the highest attainable bulk density under conventional conditions. This behavior is expected for any multivalent atomic ion and will be a limitation for any theory based on a dielectric equation of state.^{12,13,30} From Table 6, it is obvious that large changes in the predicted free energies of solvation occur only in low-dielectric regions. This result is expected due to the inverse dependence on dielectric constant (eqs 1 and 9). The error in free energy introduced by assuming $\rho^{\text{loc}} = \rho^{\max}$ in the first solvation shell is evidently negligible for temperatures as high as 900 K for densities from 0.1 to 0.5 g/cm^3 .

Free energies of solvation for individual ions cannot be measured experimentally in solution because of the physical impossibility of isolating charged species. Therefore, the solvation free energies of electrolytes composed of positive and negative species are used to evaluate the CS model. Since calculations are at infinite dilution, the free energy of solvation of the electrolyte may be computed as the sum of the free energies of solvation of its constituent ions. The CS model is compared to experiment and to the simpler Born model (eq 1). The Born radius used here will be set to the inner radius of the CS model,²³ so that these models may be compared with each other and to simulation in a consistent manner.

The experimental solvation free energies are inferred from Tanger and Pitzer's semicontinuum model for ion hydration.¹⁸ The model of Tanger and Pitzer, henceforth referred to as T-P, contains empirical parameters which are fit to give accurate agreement with a regression of experimental data compiled by Tanger and Helgeson.⁵¹ The data employed in the regressions come from heat capacities, specific heats of solution, apparent molar volumes, and compressibilities that were measured at T

TABLE 7: Solvation Thermodynamics for LiF in Water at (a) 673 K and (b) 768 K from Ref 18

ρ (g/cm ³)	P (bar)	ΔV_m^{solv} (cm ³ /mol)	ΔV^{solv} (cm ³ /mol)	ΔG_m^{solv} (kcal/mol)	ΔG^{solv} (kcal/mol)	ΔA^{solv} (kcal/mol)
(a) 673 K						
0.500	371	-1332	-1550	-194	-203	-189
0.350	298	-12 422	-13 851	-187	-195	-97
0.014	41	-16 665	-19 564	-92	-91	-72
(a) 768 K						
0.500	882	-619	-711	-187	-198	-183
0.350	600	-2518	-2798	-179	-189	-148
0.290	527	-3916	-4299	-174	-183	-129
0.014	49	-12 941	-15 639	-84	-83	-65

≤ 350 °C. Later, the Tanger and Helgeson model was extended to higher temperatures through the use of dissociation constants obtained through conductance measurements.⁵² Their regression of data was incorporated into a program called SUPCRT and its successor SUPCRT92, which is designed to calculate thermodynamic properties from 1 to 5000 bar and 0 to 1000 °C.⁸ The authors of SUPCRT92 observe that the calculation of the Gibbs free energies of formation of charged species is limited to $\rho \geq 0.35$ g/cm³, and to $T \leq 350$ or ≥ 400 °C for $P < 500$ bar.⁸ These excluded regions are of great interest in this work. Experimental data for temperatures above 350 °C are based largely on dissociation constants inferred from conductance measurements; these constants are subject to errors resulting from limitations imposed by the model of ion conductance used in analysis.⁵³ These experimental data, however, are the only available sources known to us and are therefore used as a basis for comparison as a matter of necessity.

Tanger and Pitzer model the change in Gibbs free energy and volume for the solvation process of transferring an electrolyte from a hypothetical 1 bar ideal gas-phase to a hypothetical 1 *m* ideal solution; these quantities, which we shall refer to as ΔG_m^{solv} and ΔV_m^{solv} , respectively, are given by eqs 12 and 18 of ref 18. However, in our work, we find ΔA^{solv} , which is the change in Helmholtz free energy for the solvation process of transferring an ion from an ideal gas phase to an ideal liquid solution of the same density. The following expressions relate ΔA^{solv} to ΔG_m^{solv} and ΔV_m^{solv} :

$$\Delta G^{\text{solv}} = \Delta G_m^{\text{solv}} - 2RT \ln \left(\frac{83.12\rho T}{1000} \right) \quad (10)$$

$$\Delta V^{\text{solv}} = \Delta V_m^{\text{solv}} - 2RT\beta \quad (11)$$

and

$$\Delta A^{\text{solv}} = \Delta G^{\text{solv}} - P\Delta V^{\text{solv}} \quad (12)$$

where ρ is the solvent bulk density in g/cm³, T is the temperature in K, and β is the isothermal compressibility of water obtained from ref 54. The thermodynamic quantities ΔV_m^{solv} and ΔG_m^{solv} obtained from the Tanger and Pitzer equations¹⁸ which are used to find ΔV^{solv} , ΔG^{solv} , and ultimately ΔA^{solv} are shown for LiF in water at 673 and 768 K in Table 7.

The density dependence of ΔA^{solv} for LiF and NaCl at 673 and 768 K is shown in Figure 7; the trends shown here for LiF and NaCl are representative of results we have obtained for other 1:1 electrolyte pairs. The Langmuir parameters from Table 3 and the *a* and *b* values from Table 2 are used in the CS model calculations. The CS model gives more negative free energies of solvation than the Born model because $\rho^{\text{loc}} \geq \rho$ and thus $\epsilon^{\text{loc}} \geq \epsilon$. At bulk densities > 0.5 g/cm³, where differences between ρ^{loc} and ρ become less important, the CS model essentially reduces to the Born model. At 673 K, the Born and CS models

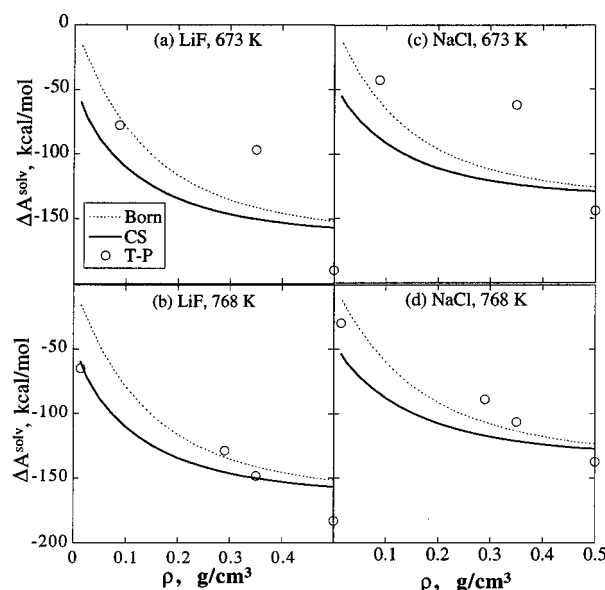


Figure 7. Free energy of solvation of LiF and NaCl in water at (a, c) 673 K and (b, d) 768 K versus solvent bulk density according to Born continuum model, concentric shell (CS) model, and Tanger and Pitzer¹⁸ (T-P) data.

predict that the concavity is upward, whereas the Tanger and Pitzer model apparently predicts the opposite.

The unexpected downward concavity for the latter model is likely due to the large uncertainty in ΔV^{solv} and ΔG^{solv} near the critical point of water. It is also due to the lack of experimental data in the lower density range. For an ion at infinite dilution, both ΔV^{solv} and ΔG^{solv} diverge at the critical point of the solvent. Hence, extrapolation of finite concentration data to infinite dilution, which is required for the T-P free energies, is difficult.⁵⁵ Because water is highly compressible at 673 K, ΔV^{solv} is large and negative, leading to large differences between ΔA^{solv} and ΔG^{solv} . The variation of Helmholtz free energy with density should be regular,⁵⁵ as it is for the CS and Born models.

In ambient water where the density is high, the CS model does not agree with experiment for ΔA^{solv} of LiF or NaCl, when the simulation values of the inner and outer radii are used. This is not surprising since, for the chloride ion, free energies from the CS model have been shown to agree very well with free energies from MD free energy perturbation at low and moderate densities, but not at high densities, e.g., in ambient water.²³ The assumption of a step function for the dielectric profile and an equation of state approach become less valid as density increases due to the importance of the structured solvation shells. Further improvement of the continuum model would need to include a spatially varying dielectric profile that better resembles the actual dielectric response of the solvent.

3.4. Compressible Continuum Model. In the compressible continuum model of Wood et al.,^{12,13,56,57} the bulk equation of state of the solvent (which inherently includes the effects of compressibility) is applied in a local fashion to an expression for the electric field, derivable from Poisson's equation, to determine self-consistently the solvent density at each point in space and thereby the electrostatic contribution to solvation free energy. Here we illustrate how the model of Wood et al. compares to simulation results at some representative state points for Cl⁻ in SCW. For our compressible continuum calculations, we implement the model presented in refs 12 and 13. It should be noted that in this presentation, we have chosen not to include the formulation of ref 56, in which corrections to the compressibility are added as a result of the electric field.

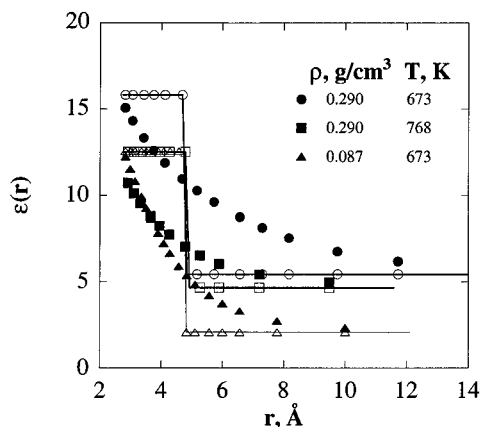


Figure 8. Dielectric profiles given by Wood's model (filled symbols) and concentric shell (CS) model (open symbols and lines) for Cl^- in water at three supercritical conditions. In these results, the Langmuir constant K is not assumed to be zero.

Two external physical descriptions of the solvent must be provided to complete the solution for the compressible continuum model: an experimental (or theoretical) evaluation of the equation of state for the bulk dielectric constant and for the isothermal compressibility of the solvent. Since this continuum model is being compared to simulation, we use the dielectric constant which was fit to simulation data for the extended simple point charge (SPC/E) model of water.⁵⁸ For the calculation of the isothermal compressibility, we use the result given by Helgeson.⁵⁴

Dielectric profiles obtained from the compressible continuum model for Cl^- in water at three conditions are shown in Figure 8 along with step dielectric profiles from the concentric shell (CS) model. The values for ρ^{max} and K used in this comparison are shown in Table 5; because a nonzero value for K is used, the local dielectric constant depends on solvent density. Both profiles asymptotically approach the bulk dielectric value as the distance from the ion increases. Under these conditions, the Wood and CS profiles have roughly the same value at the inner boundary of the first solvation shell. According to these profiles, the Wood model is expected to predict less solvation within the first shell in comparison to the CS model but greater contributions to solvation from greater distances. Both the first shell and the region beyond the first shell make important contributions to the free energy.

In Figure 9, isochores of ΔA^{solv} for Cl^- in water from 673 to 1073 K are displayed for the Born, CS, and Wood models and compared to values from MD simulations. (A comparison of the CS model with the Born model and MD simulations was made previously in ref 23.) The same ion radius is used for all three models and the simulations. In comparison to the Born model, the CS and Wood models provide far better agreement with simulation at all but the highest temperatures shown. At $\rho = 0.29 \text{ g/cm}^3$, ΔA^{solv} from simulation changes less than 10 kcal/mol over this broad temperature range, and the CS and Wood models both succeed at tracking the simulation data. Although the dielectric profiles at this density appear different (Figure 8), the differences in $1/\epsilon(r)$ are not significant when integrated to give ΔA^{solv} . For the isochore $\rho = 0.087 \text{ g/cm}^3$, ΔA^{solv} from simulation changes by more than 15 kcal/mol, and the CS and Wood models differ more from one another at 0.087 g/cm^3 than at 0.29 g/cm^3 due to the lower bulk dielectric constant. Although the CS model underpredicts the solvation free energies in the near-critical region, even here the CS model differs by less than 5 kcal/mol from the simulation values and follows the trend of the simulation data fairly well. For $\rho = 0.087 \text{ g/cm}^3$, the Wood model provides better performance at

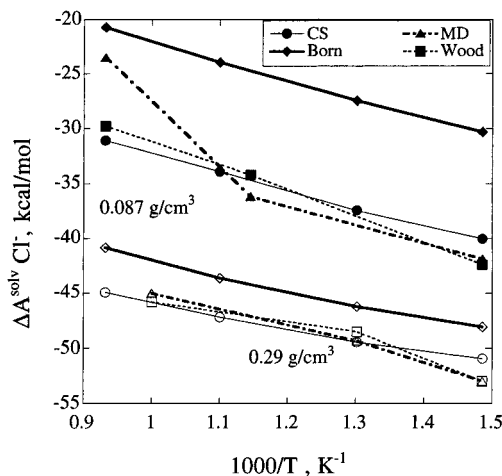


Figure 9. Comparison of the free energy of solvation for Cl^- in SCW at solvent densities of 0.087 g/cm^3 (filled symbols) and 0.29 g/cm^3 (open symbols) as given by Wood's model (with $a = 2.8 \text{ \AA}$), the Born model (with $a = 2.8 \text{ \AA}$), the concentric shell (CS) model, and MD simulations.

modeling the simulation data (within 2 kcal/mol) for all temperatures except the highest shown (1073 K). Thus, a larger contribution of shells outside the first to ΔA^{solv} , as supplied by the Wood profile, can be advantageous, although the results of the models are fairly similar. It should be noted also that excellent agreement between Wood's model extended to non-spherical molecules and MD simulation has been demonstrated for the solvation thermodynamics of an $\text{S}_{\text{N}}2$ reaction in supercritical water³⁰ at three state points: 647 K, 0.485 g/cm^3 ; 666 K, 0.165 g/cm^3 ; and 841 K, 0.162 g/cm^3 .

Over the entire range in Figure 9, the slope of ΔA^{solv} versus $1/T$ is similar for the CS, Wood, and Born models, despite the very large change in the isothermal compressibility of water. At a T_r of 1.6, both the CS and Wood models predict a more negative ΔA^{solv} than the Born model due to the high local density (Figure 5). Here the compressibility is large compared to a liquid, but small compared to a near-critical fluid. Therefore, a high compressibility is not required to achieve a high local density, as is evident in the pair correlation functions from simulation²⁹ and from the Wood model even up to 723 K.^{20,57} High local densities, for bulk densities well below the critical density, are consistent with the Langmuir model, as has been shown for nonelectrolytes in supercritical fluids such as CO_2 .^{24–28}

We have demonstrated quantitatively that a “locally inhomogeneous” or “microheterogeneous” density must be accounted for in the supercritical regime, except at the most extreme conditions of high temperature or rarefaction or in some cases of iso-Coulombic reactions.⁵⁹ Thus, continuum models with the additional requirement of an explicitly spatially dependent density distribution are desirable. The comparison above indicates that the free energy is not sensitive to this profile, except in the near-critical region.

4. Conclusions

The Langmuir adsorption analogy applied to local solvent densities about ionic solutes is quantified and shown to model simulation data for density quite accurately. Langmuir parameters corresponding to a maximum local density, ρ^{max} , and desorption constant, K , are derived for alkali and alkaline-earth metal ions and halide anions. Results show that the parameter ρ^{max} is insensitive to temperature and well correlated with the solute–water contact distance. Further, the parameter K may

be effectively approximated as zero for the purpose of calculating free energies of solvation. Hence, for spherical ionic species, local densities and ΔA^{solv} may be predicted from the surface field without the need for additional computer simulation data. Because the CS model is based on ΔA^{solv} , it is not subject to the large uncertainties present in ΔG^{solv} and ΔV^{solv} in regions where water is highly compressible. Additional experimental data are needed in the range 350–450 °C in order to test further the reliability of models for ΔA^{solv} .

The dielectric profile of Wood et al. appears to be a modest improvement over the single-step profile in the CS model due to the excess solvation versus a uniform continuum beyond the first solvation shell, although both models agree reasonably well with simulation for the case considered here. Comparative results for other solutes are certainly of interest. In this context, a consideration of a hybrid model is potentially valuable. It is worth noting in conclusion that both the model of Wood et al. and the CS model are sufficiently simple that they could be readily implemented in engineering applications.

Acknowledgment. We gratefully acknowledge support from the U.S. Army for a University Research Initiative Grant (30374-CH-URI) and an AASERT grant (DAAH 04-95-1-0649), from the Department of Energy (DE-FG07-96ER14687), from the R. A. Welch Foundation (F-0761, F-1319), from the Separations Research Program at the University of Texas, and from the National Science Foundation for a Graduate Research Fellowship awarded to L.W.F.

References and Notes

- (1) Born, M. Z. *Phys.* **1920**, *1*, 45–48.
- (2) Rashin, A. A.; Honig, B. J. *Phys. Chem.* **1985**, *89*, 5588–5593.
- (3) Gilson, M. K.; Sharp, K. A.; Honig, B. H. *J. Comput. Chem.* **1987**, *9*, 327–335.
- (4) Jayaram, B.; Fine, R.; Sharp, K.; Honig, B. J. *Phys. Chem.* **1989**, *93*, 4320–4327.
- (5) Sitkoff, D.; Sharp, K. A.; Honig, B. J. *Phys. Chem.* **1994**, *98*, 1978–1988.
- (6) Mesmer, R. E.; Palmer, D. A.; Simonson, J. M. In *Activity Coefficients in Electrolyte Solutions*, 2nd ed.; Pitzer, K. S., Ed.; CRC Press: Boca Raton, FL, 1991; pp 491–525.
- (7) Levelt Sengers, J. M. H. In *Supercritical Fluid Technology: Reviews in Modern Theory and Applications*; Bruno, T. J., Ely, J. F., Eds.; CRC Press: Boca Raton, FL, 1991; pp 1–56.
- (8) Johnson, J. W.; Oelkers, E. H.; Helgeson, H. C. *Comput. Geosci.* **1992**, *18*, 899–947.
- (9) Laidler, K. J.; Muirhead-Gould, J. S. *Trans. Faraday Soc.* **1967**, *63*, 953–957.
- (10) Goldstein, R. A.; Hay, P. F.; Kozak, J. J. *J. Chem. Phys.* **1975**, *62*, 285–291.
- (11) Abraham, M. H.; Liszi, J.; Mészáros, L. *J. Chem. Phys.* **1978**, *70*, 2491–2496.
- (12) Wood, R. H.; Quint, J. R.; Grolier, J.-P. E. *J. Phys. Chem.* **1981**, *85*, 3944–3949.
- (13) Quint, J. R.; Wood, R. H. *J. Phys. Chem.* **1985**, *89*, 380–384.
- (14) Ehrenson, S. J. *Comput. Chem.* **1989**, *10*, 77–93.
- (15) Bontha, J. R.; Pintauro, P. N. *J. Phys. Chem.* **1992**, *96*, 7778–7782.
- (16) Cossi, M.; Mennucci, B.; Tomasi, J. *Chem. Phys. Lett.* **1994**, *228*, 165–170.
- (17) Luo, H.; Tucker, S. C. *J. Phys. Chem.* **1996**, *100*, 11165–11174.
- (18) Tanger, J. C., IV; Pitzer, K. S. *J. Phys. Chem.* **1989**, *93*, 4941–4951.
- (19) Gupta, R. B.; Johnston, K. P. *Fluid Phase Equilib.* **1994**, *99*, 135–151.
- (20) Tucker, S. C.; Gibbons, E. M. In *Structure and Reactivity in Aqueous Solution: Characterization of Chemical and Biological Systems*; Truhlar, D. G., Cramer, C. J., Eds.; American Chemical Society: Washington, DC, 1994; Vol. 568, pp 196–211.
- (21) Luo, H.; Tucker, S. C. *J. Am. Chem. Soc.* **1995**, *117*, 11359–11360.
- (22) Bennett, G. E.; Johnston, K. P.; Rossky, P. J. *J. Phys. Chem.* **1995**, *99*, 16136–16143.
- (23) Johnston, K. P.; Bennett, G. E.; Balbuena, P. B.; Rossky, P. J. *J. Am. Chem. Soc.* **1996**, *118*, 6746–6752.
- (24) Kajimoto, O.; Futakami, M.; Kobayashi, T.; Yamasaki, K. *J. Phys. Chem.* **1988**, *92*, 1347–1352.
- (25) Subramanian, R.; Pyada, H.; Lira, C. T. *Ind. Eng. Chem. Res.* **1995**, *34*, 3830–3837.
- (26) Knutsen, B. L.; Tomasko, D. L.; Eckert, C. A.; Debenedetti, P. G.; Chialvo, A. A. In *Supercritical Fluid Technology*; Bright, F. V., McNally, M. E. P., Eds.; American Chemical Society: Washington, DC, 1992; Vol. 488, pp 60–72.
- (27) Sun, Y.-P.; Bunker, C. E.; Hamilton, N. B. *Chem. Phys. Lett.* **1993**, *210*, 111–117.
- (28) Carlier, C.; Randolph, T. W. *AIChE J.* **1993**, *39*, 876–884.
- (29) Flanagan, L. W.; Balbuena, P. B.; Johnston, K. P.; Rossky, P. J. *J. Phys. Chem.* **1995**, *99*, 5196–5205.
- (30) Luo, H.; Tucker, S. C. *J. Phys. Chem. B* **1997**, *101*, 1063–1071.
- (31) Berendsen, H. J. C.; Postma, J. P. M.; van Gunsteren, W. F.; Hermans, J. In *Intermolecular Forces*; Pullman, B., Ed.; D. Reidel: Dordrecht, Holland, 1981; pp 331–342.
- (32) Guissani, Y.; Guillot, B. *J. Chem. Phys.* **1993**, *98*, 8221–8235.
- (33) Mountain, R. D.; Wallqvist, A. A collection of results for the SPC/E water model. National Institute of Standards and Technology, 1996.
- (34) Kistenmacher, H.; Popkie, H.; Clementi, E. *J. Chem. Phys.* **1973**, *59*, 5842–5848.
- (35) Dzidic, I.; Kebarle, P. *J. Phys. Chem.* **1970**, *74*, 1466–1474.
- (36) Arshadi, M.; Yamdagni, R.; Kebarle, P. *J. Phys. Chem.* **1970**, *74*, 1475–1482.
- (37) Kollman, P. A.; Kuntz, I. D. *J. Am. Chem. Soc.* **1972**, *94*, 9236–9237.
- (38) de Leeuw, S. W.; Perram, J. W.; Smith, E. R. *Proc. R. Soc. London* **1980**, *A 373*, 27–56.
- (39) Belhadj, M.; Alper, H. E.; Levy, R. M. *Chem. Phys. Lett.* **1991**, *179*, 13–20.
- (40) Cochran, H. D.; Lee, L. L. In *Supercritical Fluid Science and Technology*; Johnston, K. P., Penninger, J. M. L., Eds.; American Chemical Society: Washington, DC, 1989; Vol. 406, pp 27–38.
- (41) Cummings, P. T.; Chialvo, A. A.; Cochran, H. D. *Chem. Eng. Sci.* **1994**, *49*, 2735–2748.
- (42) Balbuena, P. B.; Flanagan, L. W.; Johnston, K. P.; Rossky, P. J. In *Physical Chemistry of Aqueous Systems: Meeting the Needs of Industry*; White Jr., H. J., Senger, J. V., Neumann, D. B., Bellows, J. C., Eds.; Begell House: New York, 1995; pp 595–601.
- (43) Balbuena, P. B.; Johnston, K. P.; Rossky, P. J. *J. Phys. Chem.* **1996**, *100*, 2706–2715.
- (44) Chandrasekhar, J.; Spellmeyer, D. C.; Jorgensen, W. L. *J. Am. Chem. Soc.* **1984**, *106*, 903–910.
- (45) Enderby, J. E.; Neilson, G. W. In *Water: A Comprehensive Treatise*; Franks, F., Ed.; Plenum Press: New York, 1979; Vol. 6, pp 1–46.
- (46) Enderby, J. E.; Neilson, G. W. *Rep. Prog. Phys.* **1981**, *44*, 593–653.
- (47) Beveridge, D. L.; Schnuelle, G. W. *J. Phys. Chem.* **1975**, *79*, 2562–2566.
- (48) Lee, L. L. *Molecular Thermodynamics of Nonideal Fluids*; Butterworth: Boston, 1988.
- (49) McQuarrie, D. A. *Statistical Mechanics*; Harper Collins: New York, 1976.
- (50) Uematsu, M.; Franck, E. U. *J. Phys. Chem. Ref. Data* **1980**, *9*, 1291–1306.
- (51) Tanger, J. C., IV; Helgeson, H. C. *Am. J. Sci.* **1988**, *288*, 19–98.
- (52) Shock, E. L.; Oelkers, E. H.; Johnson, J. W.; Sverjensky, D. A.; Helgeson, H. C. *J. Chem. Soc., Faraday Trans.* **1992**, *88*, 803–826.
- (53) Balbuena, P. B. Ph.D. Thesis, The University of Texas at Austin, 1996.
- (54) Helgeson, H. C.; Kirkham, D. H. *Am. J. Sci.* **1974**, *274*, 1089–1198.
- (55) Levelt Sengers, J. M. H.; Harvey, A. H.; Crovetto, R.; Gallagher, J. S. *Fluid Phase Equilib.* **1992**, *81*, 85–107.
- (56) Wood, R. H.; Quint, J. R. *J. Phys. Chem.* **1989**, *93*, 936–937.
- (57) Wood, R. H.; Carter, R. W.; Quint, J. R.; Majer, V.; Thompson, P. T.; Boccio, J. R. *J. Chem. Thermodyn.* **1994**, *26*, 225–249.
- (58) Neumann, M. In *Physical Chemistry of Aqueous Systems: Meeting the Needs of Industry*; White, H. J., Jr., Sengers, J. V., Neumann, D. B., Bellows, J. C., Eds.; Begell House: New York, 1995; pp 261–268.
- (59) Balbuena, P. B.; Johnston, K. P.; Rossky, P. J. *J. Phys. Chem.* **1996**, *100*, 2716–2722.
- (60) Rosseinsky, D. R. *Chem. Rev.* **1965**, *65*, 467–490.